

PROBLEMS

1. Equivalent electrical circuit	391
2. Rotating coordinate system	391
3. Hyperfine effects on ESR in metals	391
4. FMR in the anisotropy field	391
5. Exchange frequency resonance	391
6. Rf saturation	391

391

CHAPTER 13: MAGNETIC RESONANCE

In this chapter we discuss dynamical magnetic effects associated with the spin angular momentum of nuclei and of electrons. The principal phenomena are often identified in the literature by their initial letters, such as

NMR: nuclear magnetic resonance

NQR: nuclear quadrupole resonance

EPR or ESR: electron paramagnetic or spin resonance (Fig. 1)

FMR: ferromagnetic resonance

SWR: spin wave resonance (ferromagnetic films)

AFMR: antiferromagnetic resonance

CESR: conduction electron spin resonance

The information that can be obtained about solids by resonance studies may be categorized:

- Electronic structure of single defects, as revealed by the fine structure of the absorption.
- Motion of the spin or of the surroundings, as revealed by changes in the line width.
- Internal magnetic fields sampled by the spin, as revealed by the position of the resonance line (chemical shift; Knight shift).
- Collective spin excitations.

It is best to discuss NMR as a basis for a brief account of the other resonance experiments. A great impact of NMR has been in organic chemistry and biochemistry, where NMR provides a powerful tool for the identification and the structure determination of complex molecules. This success is due to the extremely high resolution attainable in diamagnetic liquids. A major medical application of NMR is magnetic resonance imaging (MRI), which allows the resolution in 3D of abnormal growths, configurations, and reactions in the whole body.

NUCLEAR MAGNETIC RESONANCE

We consider a nucleus that possesses a magnetic moment μ and an angular momentum $\hbar\mathbf{I}$. The two quantities are parallel, and we may write

$$\mu = \gamma \hbar \mathbf{I} ; \quad (1)$$

the magnetogyric ratio γ is constant. By convention \mathbf{I} denotes the nuclear angular momentum measured in units of \hbar .

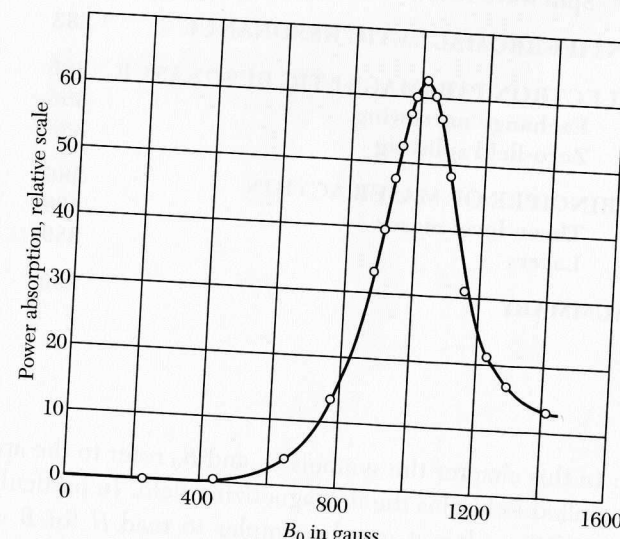


Figure 1 Electron spin resonance absorption in MnSO_4 at 298 K at 2.75 GHz, after Zavoisky.

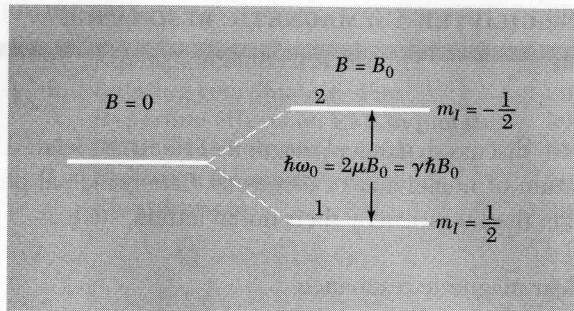


Figure 2 Energy level splitting of a nucleus of spin $I = \frac{1}{2}$ in a static magnetic field B_0 .

The energy of interaction with the applied magnetic field is

$$U = -\boldsymbol{\mu} \cdot \mathbf{B}_a ; \quad (2)$$

if $\mathbf{B}_a = B_0 \hat{\mathbf{z}}$, then

$$U = -\mu_{\tilde{z}} B_0 = -\gamma \hbar B_0 I_z \quad . \quad (3)$$

The allowed values of $I_{\tilde{z}}$ are $m_I = I, I-1, \dots, -I$, and $U = -m_I \gamma \hbar B_0$.

In a magnetic field a nucleus with $I = \frac{1}{2}$ has two energy levels corresponding to $m_I = \pm \frac{1}{2}$, as in Fig. 2. If $\hbar\omega_0$ denotes the energy difference between the two levels, then $\hbar\omega_0 = \gamma\hbar B_0$ or

$$\omega_0 = \gamma B_0 \quad . \quad (4)$$

This is the fundamental condition for magnetic resonance absorption.

For the proton¹ $\gamma = 2.675 \times 10^4 \text{ s}^{-1} \text{ gauss}^{-1} = 2.675 \times 10^8 \text{ s}^{-1} \text{ tesla}^{-1}$, so that

$$\nu(\text{MHz}) = 4.258 B_0(\text{kilogauss}) = 42.58 B_0(\text{tesla}) . \quad (4a)$$

where ν is the frequency. One tesla is precisely 10^4 gauss. Magnetic data for selected nuclei are given in Table 1. For the electron spin

$$\nu(\text{GHz}) = 2.80 B_0(\text{kilogauss}) = 28.0 B_0(\text{tesla}) . \quad (4b)$$

¹The magnetic moment μ_p of the proton is 1.4106×10^{-23} erg G⁻¹ or 1.4106×10^{-26} J T⁻¹, and $\gamma = 2\mu_p/h$. The **nuclear magneton** μ_n is defined as $e\hbar/2M_p c$ and is equal to 5.0509×10^{-24} erg G⁻¹ or 5.0509×10^{-27} J T⁻¹; thus $\mu_n = 2.793$ nuclear magnetons.

Table I Nuclear magnetic resonance data

For every element the most abundant magnetic isotope is shown. After Varian Associates NMR Table.

H ¹	Li ⁷	Be ⁹	B ¹¹	C ¹³	N ¹⁴	O ¹⁷	F ¹⁹	Ne ²¹	Kr ³³	Xe ¹²⁹								
1/2 99.98 2.792	3/2 92.57 100. 3.256 -1.177	3/2 100. 10.05 0.855 0.855	3/2 81.17 2.688	1/2 1.108 0.702	1 99.64 0.404	5/2 0.04 -1.893	1/2 100.	3/2 3/2 3/2 3/2 3/2	3/2 0.257 -0.662 -2.627 -2.127	3/2 100. 75.4 0.821 1.127								
Na ²³	Mg ²⁵	Sc ⁴⁵	Ti ⁴⁷	V ⁵¹	Mn ⁵⁵	Fe ⁵⁷	Co ⁵⁹	Ni ⁶¹	Cu ⁶³	Zn ⁶⁷	Ge ⁷³	As ⁷⁵	Se ⁷⁷	Br ⁷⁹				
3/2 5/2 100. 2.216	5/2 10.05 0.855	7/2 100. 7.75 -1.315	5/2 ~100. 9.54 0.787 0.787	3/2 100. 1.39 5.139 5.139	5/2 100. 1.39 0.474 0.474	1/2 2.245 0.090 0.746 0.746	7/2 100. 1.25 2.221 2.221	3/2 1.25 0.746 0.874 0.874	3/2 69.09 0.877 0.877	5/2 4.12 0.877 0.877	9/2 60.2 1.00 0.877	3/2 7.61 100. 0.877	1/2 7.61 100. 0.877	3/2 50.57 11.55 -0.967				
K ³⁹	Ca ⁴³	Sc ⁴⁵	Ti ⁴⁷	V ⁵¹	Cr ⁵³	Mn ⁵⁵	Fe ⁵⁷	Co ⁵⁹	Ni ⁶¹	Cu ⁶³	Ge ⁷³	As ⁷⁵	Se ⁷⁷	Br ⁷⁹				
3/2 93.08 0.391	7/2 0.13 -1.315	7/2 100. 7.75 4.749 4.749	5/2 ~100. 9.54 0.787 0.787	3/2 100. 1.39 5.139 5.139	5/2 100. 1.39 0.474 0.474	1/2 2.245 0.090 0.746 0.746	7/2 100. 1.25 2.221 2.221	3/2 1.25 0.746 0.874 0.874	5/2 69.09 0.877 0.877	3/2 4.12 0.877 0.877	9/2 60.2 1.00 0.877	3/2 7.61 100. 0.877	1/2 7.61 100. 0.877	3/2 50.57 11.55 -0.967				
Rb ⁸⁵	Sr ⁸⁷	Y ⁸⁹	Zr ⁹¹	Nb ⁹³	Mo ⁹⁵	Tc	Ru ¹⁰¹	Rh ¹⁰³	Pd ¹⁰⁵	Ag ¹⁰⁷	Cd ¹¹¹	In ¹¹⁵	Sb ¹²¹	Te ¹²⁵	I ¹²⁷			
5/2 72.8 1.348	9/2 7.02 1.089	1/2 100. 0.137	5/2 100. 11.23 1.298 1.298	9/2 100. 100. 1.910 1.910	5/2 100. 100. 0.910 0.910	5/2 15.78 16.98 0.69 0.69	1/2 100. 22.23 -0.69 -0.69	1/2 22.23 51.35 -0.57 -0.57	1/2 12.86 12.86 -0.113 -0.113	9/2 9.68 8.68 -0.582 -0.582	1/2 8.68 8.68 -0.507 -0.507	5/2 12.86 12.86 -0.1041 -0.1041	1/2 5.507 5.507 -0.342 -0.342	5/2 5.507 5.507 -0.342 -0.342	1/2 5.507 5.507 -0.342 -0.342	5/2 5.507 5.507 -0.342 -0.342		
Cs ¹³³	Ba ¹³⁷	La ¹³⁹	Hf ¹⁷⁷	Ta ¹⁸¹	W ¹⁸³	Re ¹⁸⁷	Os ¹⁸⁹	Ir ¹⁹³	Pt ¹⁹⁵	Au ¹⁹⁷	Hg ¹⁹⁹	Tl ²⁰⁵	Pb ²⁰⁷	Bi ²⁰⁹	Po ²¹⁰	At ²¹¹	Rn ²¹²	
7/2 100. 2.564	3/2 11.32 0.931	7/2 99.9 2.761	7/2 18.39 1.00 0.61	7/2 100. 14.28 3.176 3.176	5/2 100. 62.93 16.1 0.651 0.651	1/2 100. 61.5 33.7 0.17	3/2 100. 61.5 33.7 0.600 0.600	1/2 100. 61.5 33.7 0.144 0.144	3/2 100. 61.5 33.7 0.144 0.144	1/2 100. 61.5 33.7 0.144 0.144	1/2 100. 61.5 33.7 0.144 0.144	9/2 70.48 70.48 70.48 1.612 1.612	1/2 21.11 21.11 21.11 0.584 0.584	1/2 100. 100. 100. 4.039 4.039	9/2 21.11 21.11 21.11 1.612 1.612	1/2 100. 100. 100. -0.20 -0.20	5/2 22.82 22.82 22.82 -0.677 -0.677	1/2 100. 100. 100. -0.20 -0.20
Fr	Ra	Ac	Ce ¹⁴¹ *	Pr ¹⁴¹	Nd ¹⁴³	Pm	Sm ¹⁵¹	Eu ¹⁵³	Gd ¹⁵⁷	Tb ¹⁵⁹	Dy ¹⁶³	Ho ¹⁶⁵	Er ¹⁶⁷	Tm ¹⁶⁹	Yb ¹⁷³	Lu ¹⁷⁵		
			7/2 -	5/2 100.	7/2 12.20	5/2 -0.68	7/2 15.07	5/2 52.23	3/2 15.64	3/2 100.	5/2 24.97	7/2 100.	5/2 24.97	1/2 100.	5/2 22.82	7/2 100.		
Th	Pa	U	Np	Pu	Am	Cm	Bk	Cf	Es	Fm	Md	No	Lr					

Equations of Motion

The rate of change of angular momentum of a system is equal to the torque that acts on the system. The torque on a magnetic moment μ in a magnetic field \mathbf{B} is $\mu \times \mathbf{B}$, so that we have the gyroscopic equation

$$\hbar d\mathbf{I}/dt = \mu \times \mathbf{B}_a ; \quad (5)$$

or

$$d\mu/dt = \gamma\mu \times \mathbf{B}_a . \quad (6)$$

The nuclear magnetization \mathbf{M} is the sum $\sum \mu_i$ over all the nuclei in a unit volume. If only a single isotope is important, we consider only a single value of γ , so that

$$d\mathbf{M}/dt = \gamma\mathbf{M} \times \mathbf{B}_a . \quad (7)$$

We place the nuclei in a static field $\mathbf{B}_a = B_0\hat{\mathbf{z}}$. In thermal equilibrium at temperature T the magnetization will be along $\hat{\mathbf{z}}$:

$$M_x = 0 ; \quad M_y = 0 ; \quad M_z = M_0 = \chi_0 B_0 = CB_0/T , \quad (8)$$

where the susceptibility is χ_0 and the Curie constant $C = N\mu^2/3k_B$, as in Chapter 11.

The magnetization of a system of spins with $I = \frac{1}{2}$ is related to the population difference $N_1 - N_2$ of the lower and upper levels in Fig. 2: $M_z = (N_1 - N_2)\mu$, where the N 's refer to a unit volume. The population ratio in thermal equilibrium is just given by the Boltzmann factor for the energy difference $2\mu B_0$:

$$(N_2/N_1)_0 = \exp(-2\mu B_0/k_B T) . \quad (9)$$

The equilibrium magnetization is $M_0 = N\mu \tanh(\mu B_0/k_B T)$.

When the magnetization component M_z is not in thermal equilibrium, we suppose that it approaches equilibrium at a rate proportional to the departure from the equilibrium value M_0 :

$$\frac{dM_z}{dt} = \frac{M_0 - M_z}{T_1} . \quad (10)$$

In the standard notation T_1 is called the **longitudinal relaxation time** or the **spin-lattice relaxation time**.

If at $t = 0$ an unmagnetized specimen is placed in a magnetic field $B_0\hat{\mathbf{z}}$, the magnetization will increase from the initial value $M_z = 0$ to a final value $M_z = M_0$. Before and just after the specimen is placed in the field, the population N_1 will be equal to N_2 , as appropriate to thermal equilibrium in zero magnetic field. It is necessary to reverse some spins to establish the new equilibrium distribution in the field B_0 . On integrating (10):

$$\int_0^{M_z} \frac{dM_z}{M_0 - M_z} = \frac{1}{T_1} \int_0^t dt , \quad (11)$$

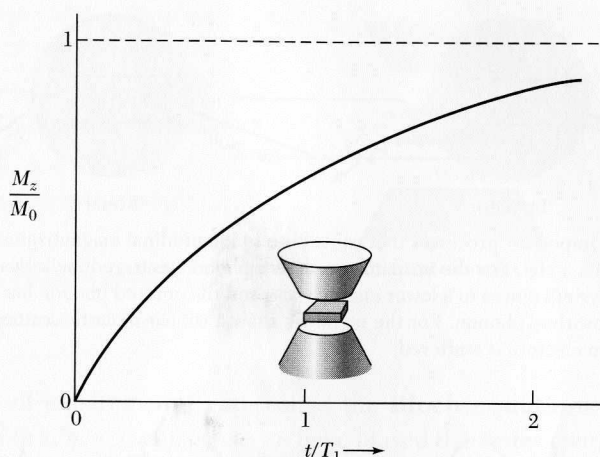


Figure 3 At time $t = 0$ an unmagnetized specimen $M_z(0) = 0$ is placed in a static magnetic field B_0 . The magnetization increases with time and approaches the new equilibrium value $M_0 = \chi_0 B_0$. This experiment defines the longitudinal relaxation time T_1 . The magnetic energy density $-\mathbf{M} \cdot \mathbf{B}$ decreases as part of the spin population moves into the lower level. The asymptotic value at $t \gg T_1$ is $-M_0 B_0$. The energy flows from the spin system to the system of lattice vibrations; thus T_1 is also called the spin-lattice relaxation time.

or

$$\log \frac{M_0}{M_0 - M_z} = \frac{t}{T_1} ; \quad M_z(t) = M_0[1 - \exp(-t/T_1)] , \quad (12)$$

as in Fig. 3. The magnetic energy $-\mathbf{M} \cdot \mathbf{B}_a$ decreases as M_z approaches its new equilibrium value.

Typical processes whereby the magnetization approaches equilibrium are indicated in Fig. 4. The dominant spin-lattice interaction of paramagnetic ions in crystals is by the phonon modulation of the crystalline electric field. Relaxation proceeds by three principal processes (Fig. 4b): direct (emission or absorption of a phonon); Raman (scattering of a phonon); and Orbach (interaction of a third state).

Taking account of (10), the z component of the equation of motion (7) becomes

$$\frac{dM_z}{dt} = \gamma(\mathbf{M} \times \mathbf{B}_a)_z + \frac{M_0 - M_z}{T_1} , \quad (13a)$$

where $(M_0 - M_z)/T_1$ is an extra term in the equation of motion, arising from the spin-lattice interactions not included in (7). That is, besides precessing about the magnetic field, \mathbf{M} will relax to the equilibrium value \mathbf{M}_0 .

If in a static field $B_0\hat{\mathbf{z}}$ the transverse magnetization component M_x is not zero, then M_x will decay to zero, and similarly for M_y . The decay occurs

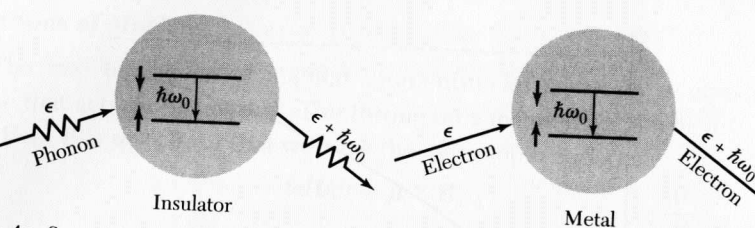


Figure 4a Some important processes that contribute to longitudinal magnetization relaxation in an insulator and in a metal. For the insulator we show a phonon scattered inelastically by the spin system. The spin system moves to a lower energy state, and the emitted phonon has higher energy by $\hbar\omega_0$ than the absorbed phonon. For the metal we show a similar inelastic scattering process in which a conduction electron is scattered.

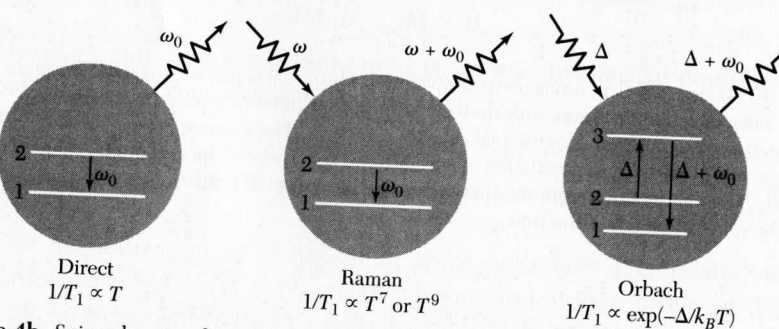


Figure 4b Spin relaxation from $2 \rightarrow 1$ by phonon emission, phonon scattering, and a two-stage phonon process. The temperature dependence of the longitudinal relaxation time T_1 is shown for the several processes.

because in thermal equilibrium the transverse components are zero. We can provide for transverse relaxation:

$$dM_x/dt = \gamma(\mathbf{M} \times \mathbf{B}_a)_x - M_x/T_2 ; \quad (13b)$$

$$dM_y/dt = \gamma(\mathbf{M} \times \mathbf{B}_a)_y - M_y/T_2 , \quad (13c)$$

where T_2 is called the **transverse relaxation time**.

The magnetic energy $-\mathbf{M} \cdot \mathbf{B}_a$ does not change as M_x or M_y changes, provided that \mathbf{B}_a is along $\hat{\mathbf{z}}$. No energy need flow out of the spin system during relaxation of M_x or M_y , so that the conditions that determine T_2 may be less strict than for T_1 . Sometimes the two times are nearly equal, and sometimes $T_1 \gg T_2$, depending on local conditions.

The time T_2 is a measure of the time during which the individual moments that contribute to M_x , M_y remain in phase with each other. Different local magnetic fields at the different spins will cause them to precess at different frequencies. If initially the spins have a common phase, the phases will become random in the course of time and the values of M_x , M_y will become zero. We can think of T_2 as a dephasing time.

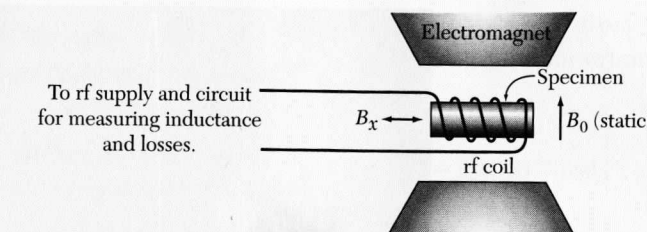


Figure 5 Schematic arrangement for magnetic resonance experiments.

The set of equations (13) are called the **Bloch equations**. They are not symmetrical in x , y , and z because we have biased the system with a static magnetic field along $\hat{\mathbf{z}}$. In experiments an rf magnetic field is usually applied along the $\hat{\mathbf{x}}$ or $\hat{\mathbf{y}}$ axis. Our main interest is in the behavior of the magnetization in the combined rf and static fields, as in Fig. 5. The Bloch equations are plausible, but not exact; they do not describe all spin phenomena, particularly not those in solids.

We determine the frequency of free precession of the spin system in a static field $\mathbf{B}_a = B_0 \hat{\mathbf{z}}$ and with $M_z = M_0$. The Bloch equations reduce to

$$\frac{dM_x}{dt} = \gamma B_0 M_y - \frac{M_x}{T_2} ; \quad \frac{dM_y}{dt} = -\gamma B_0 M_x - \frac{M_y}{T_2} ; \quad \frac{dM_z}{dt} = 0 . \quad (14)$$

We look for damped oscillatory solutions of the form

$$M_x = m \exp(-t/T') \cos \omega t ; \quad M_y = -m \exp(-t/T') \sin \omega t . \quad (15)$$

On substitution in (14) we have for the left-hand equation

$$-\omega \sin \omega t - \frac{1}{T'} \cos \omega t = -\gamma B_0 \sin \omega t - \frac{1}{T_2} \cos \omega t , \quad (16)$$

so that the free precession is characterized by

$$\omega_0 = \gamma B_0 ; \quad T' = T_2 . \quad (17)$$

The motion (15) is similar to that of a damped harmonic oscillator in two dimensions. The analogy suggests correctly that the spin system will show resonance absorption of energy from a driving field near the frequency $\omega_0 = \gamma B_0$, and the frequency width of the response of the system to the driving field will be $\Delta\omega \approx 1/T_2$. Figure 6 shows the resonance of protons in water.

The Bloch equations may be solved to give the power absorption from a rotating magnetic field of amplitude B_1 :

$$B_x = B_1 \cos \omega t ; \quad B_y = -B_1 \sin \omega t . \quad (18)$$

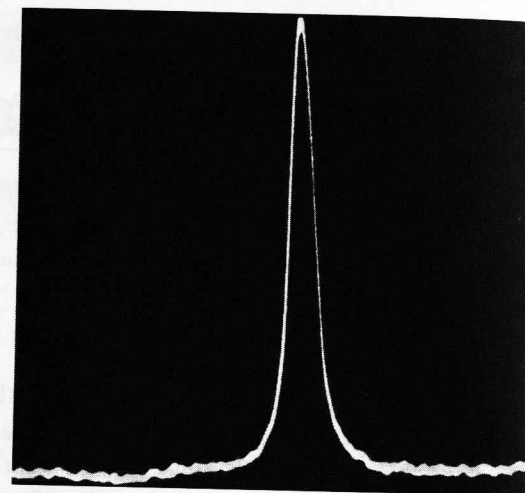


Figure 6 Proton resonance absorption in water.
(E. L. Hahn.)

After a routine calculation one finds that the power absorption is

$$(CGS) \quad \mathcal{P}(\omega) = \frac{\omega\gamma M_z T_2}{1 + (\omega_0 - \omega)^2 T_2^2} B_1^2. \quad (19)$$

The half-width of the resonance at half-maximum power is

$$(\Delta\omega)_{1/2} = 1/T_2. \quad (20)$$

LINE WIDTH

The magnetic dipolar interaction is usually the most important cause of line broadening in a rigid lattice of magnetic dipoles. The magnetic field $\Delta\mathbf{B}$ seen by a magnetic dipole μ_1 due to a magnetic dipole μ_2 at a point \mathbf{r}_{12} from the first dipole is

$$(CGS) \quad \Delta\mathbf{B} = \frac{3(\mu_2 \cdot \mathbf{r}_{12})\mathbf{r}_{12} - \mu_2 r_{12}^2}{r_{12}^5}, \quad (21)$$

by a fundamental result of magnetostatics.

The order of magnitude of the interaction is, with B_i written for ΔB ,

$$(CGS) \quad B_i \approx \mu/r^3. \quad (22)$$

The strong dependence on r suggests that close-neighbor interactions will be dominant, so that

$$(CGS) \quad B_i \approx \mu/a^3, \quad (23)$$

where a is the separation of nearest neighbors. This result gives us a measure of the width of the spin resonance line, assuming random orientation of the neighbors. For protons at 2 Å separation,

$$B_i \approx \frac{1.4 \times 10^{-23} \text{ G cm}^3}{8 \times 10^{-24} \text{ cm}^3} \approx 2 \text{ gauss} = 2 \times 10^{-4} \text{ tesla}. \quad (24)$$

To express (21), (22), and (23) in SI, multiply the right-hand sides by $\mu_0/4\pi$.

Motional Narrowing

The line width decreases for nuclei in rapid relative motion. The effect in solids is illustrated by Fig. 7: diffusion resembles a random walk as atoms jump from one crystal site to another. An atom remains in one site for an average time τ that decreases markedly as the temperature increases.

The motional effects on the line width are even more spectacular in normal liquids, because the molecules are highly mobile. The width of the proton resonance line in water is only 10^{-5} of the width expected for water molecules frozen in position.

The effect of nuclear motion on T_2 and on the line width is subtle, but can be understood by an elementary argument. We know from the Bloch equations that T_2 is a measure of the time in which an individual spin becomes dephased by one radian because of a local perturbation in the magnetic field

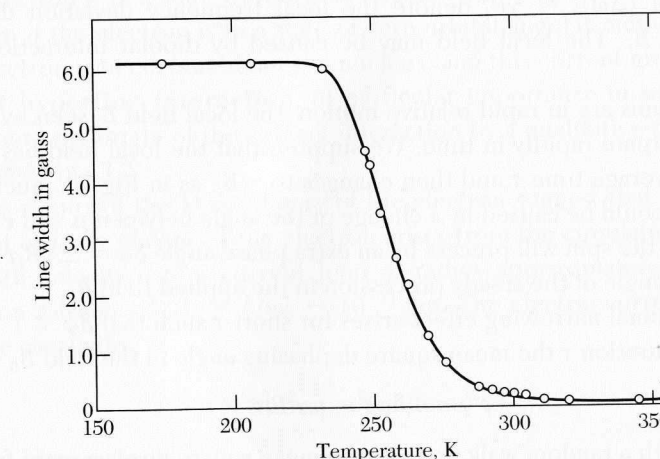


Figure 7 Effect of diffusion of nuclei on the Li^7 NMR line width in metallic lithium. At low temperatures the width agrees with the theoretical value for a rigid lattice. As the temperature increases, the diffusion rate increases and the line width decreases. The abrupt decrease in line width above $T = 230$ K occurs when the diffusion hopping time τ becomes shorter than $1/\gamma B_i$. Thus the experiment gives a direct measure of the hopping time for an atom to change lattice sites. (After H. S. Gutowsky and B. R. McGarvey.)

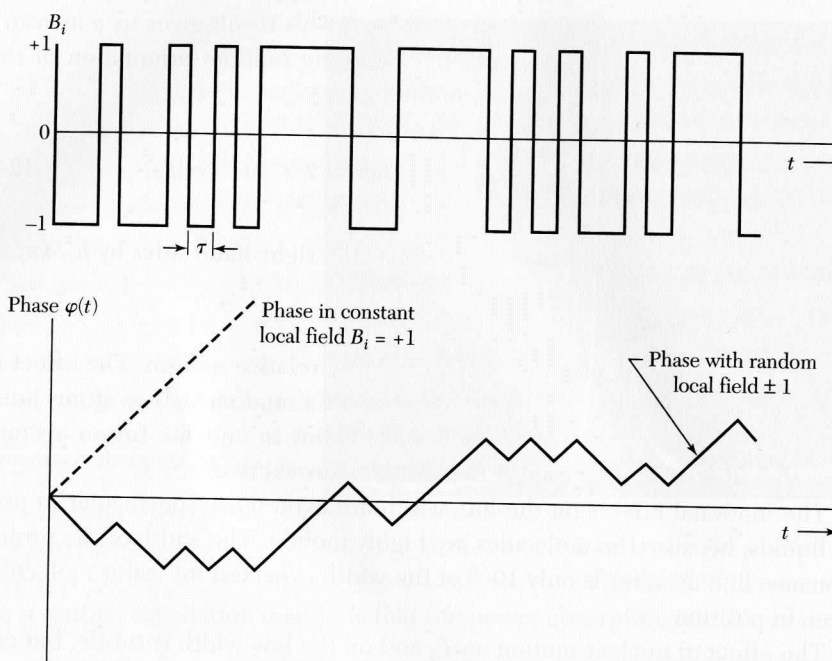


Figure 8 Phase of a spin in a constant local field, as compared with dephasing of a spin which after fixed time intervals τ hops at random among sites having local fields ± 1 .

intensity. Let $(\Delta\omega)_0 \approx \gamma B_i$ denote the local frequency deviation due to a perturbation B_i . The local field may be caused by dipolar interactions with other spins.

If the atoms are in rapid relative motion, the local field B_i seen by a given spin will fluctuate rapidly in time. We suppose that the local field has a value $+B_i$ for an average time τ and then changes to $-B_i$, as in Fig. 8a. Such a random change could be caused by a change of the angle between μ and r in (21). In the time τ the spin will precess by an extra phase angle $\delta\varphi = \pm\gamma B_i \tau$ relative to the phase angle of the steady precession in the applied field B_0 .

The motional narrowing effect arises for short τ such that $\delta\varphi \ll 1$. After n intervals of duration τ the mean square dephasing angle in the field B_0 will be

$$\langle \varphi^2 \rangle = n(\delta\varphi)^2 = n\gamma^2 B_i^2 \tau^2 , \quad (25)$$

by analogy with a random walk process: the mean square displacement from the initial position after n steps of length ℓ in random directions is $\langle r^2 \rangle = n\ell^2$.

The average number of steps necessary to dephase a spin by one radian is $n = 1/\gamma^2 B_i^2 \tau^2$. (Spins dephased by much more than one radian do not contribute to the absorption signal.) This number of steps takes place in a time

$$T_2 = n\tau = 1/\gamma^2 B_i^2 \tau , \quad (26)$$

quite different from the rigid lattice result $T_2 \cong 1/\gamma B_i$. From (26) we obtain as the line width for rapid motion with a characteristic time τ :

$$\Delta\omega = 1/T_2 = (\gamma B_i)^2 \tau , \quad (27)$$

or

$$\Delta\omega = 1/T_2 = (\Delta\omega)_0^2 \tau , \quad (28)$$

where $(\Delta\omega)_0$ is the line width in the rigid lattice.

The argument assumes that $(\Delta\omega)_0 \tau \ll 1$, as otherwise $\delta\varphi$ will not be $\ll 1$. Thus $\Delta\omega \ll (\Delta\omega)_0$. The shorter is τ , the narrower is the resonance line! This remarkable effect is known as **motional narrowing**.² The rotational relaxation time of water molecules at room temperature is known from dielectric constant measurements to be of the order of 10^{-10} s; if $(\Delta\omega)_0 \approx 10^5$ s⁻¹, then $(\Delta\omega)_0 \tau \approx 10^{-5}$ and $\Delta\omega \approx (\Delta\omega)_0^2 \tau \approx 1$ s⁻¹. Thus the motion narrows the proton resonance line to about 10^{-5} of the static width.

HYPFINE SPLITTING

The hyperfine interaction is the magnetic interaction between the magnetic moment of a nucleus and the magnetic moment of an electron. To an observer stationed on the nucleus, the interaction is caused by the magnetic field produced by the magnetic moment of the electron and by the motion of the electron about the nucleus. There is an electron current about the nucleus if the electron is in a state with orbital angular momentum about the nucleus. But even if the electron is in a state of zero orbital angular momentum, there is an electron spin current about the nucleus, and this current gives rise to the **contact hyperfine interaction**, of particular importance in solids. We can understand the origin of the contact interaction by a qualitative physical argument, given in CGS.

The results of the Dirac theory of the electron suggest that the magnetic moment of $\mu_B = e\hbar/2mc$ of the electron arises from the circulation of an electron with velocity c in a current loop of radius approximately the electron Compton wavelength, $\lambda_e = \hbar/mc \sim 10^{-11}$ cm. The electric current associated with the circulation is

$$I \sim e \times (\text{turns per unit time}) \sim ec/\lambda_e , \quad (29)$$

²The physical ideas are due to N. Bloembergen, E. M. Purcell, and R. V. Pound, Phys. Rev. 73, 679 (1948). The result differs from the theory of optical line width caused by *strong* collisions between atoms (as in a gas discharge), where a short τ gives a broad line. In the nuclear spin problem the collisions are weak. In most optical problems the collisions of atoms are strong enough to interrupt the phase of the oscillation. In nuclear resonance the phase may vary smoothly in a collision, although the frequency may vary suddenly from one value to another nearby value.

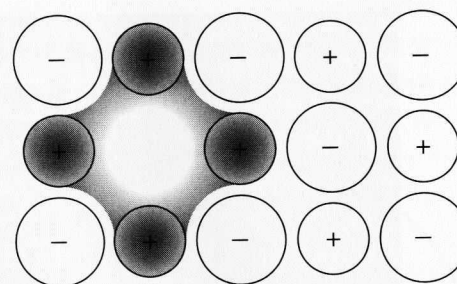


Figure 11 An *F* center is a negative ion vacancy with one excess electron bound at the vacancy. The distribution of the excess electron is largely on the positive metal ions adjacent to the vacant lattice site.

F Centers in Alkali Halides. An *F* center is a negative ion vacancy with one excess electron bound at the vacancy (Fig. 11). The wavefunction of the trapped electron is shared chiefly among the six alkali ions adjacent to the vacant lattice site, with smaller amplitudes on the 12 halide ions that form the shell of second nearest neighbors. The counting applies to crystals with the NaCl structure. If $\varphi(\mathbf{r})$ is the wavefunction of the valence electron on a single alkali ion, then in the first (or LCAO) approximation

$$\psi(\mathbf{r}) = C \sum_p \varphi(\mathbf{r} - \mathbf{r}_p), \quad (35)$$

where in the NaCl structure the six values of \mathbf{r}_p mark the alkali ion sites that bound the lattice vacancy.

The width of the electron spin resonance line of an *F* center is determined essentially by the hyperfine interaction of the trapped electron with the nuclear magnetic moments of the alkali ions adjacent to the vacant lattice site. The observed line width is evidence for the simple picture of the wavefunction of the electron. By line width we mean the width of the envelope of the possible hyperfine structure components.

As an example, consider an *F* center in KCl. Natural potassium is 93 percent K^{39} with nuclear spin $I = \frac{3}{2}$. The total spin of the six potassium nuclei at the *F* center is $I_{\max} = 6 \times \frac{3}{2} = 9$, so that the number of hyperfine components is $2I_{\max} + 1 = 19$; this is the number of possible values of the quantum number m_I . There are $(2I + 1)^6 = 4^6 = 4096$ independent arrangements of the six spins distributed into the 19 components, as in Fig. 12. Often we observe only the envelope of the absorption line of an *F* center.

Donor Atoms in Silicon. Phosphorus is a donor when present in silicon. Each donor atom has five outer electrons, of which four enter diamagnetically into the covalent bond network of the crystal, and the fifth acts as a paramagnetic center of spin $S = \frac{1}{2}$. The experimental hyperfine splitting in the strong field limit is shown in Fig. 13.

When the concentration exceeds about 1×10^{18} donors cm^{-3} , the split line is replaced by a single narrow line. This is a motional narrowing effect (Eq. 28) of the rapid hopping of the donor electrons among many donor atoms. The

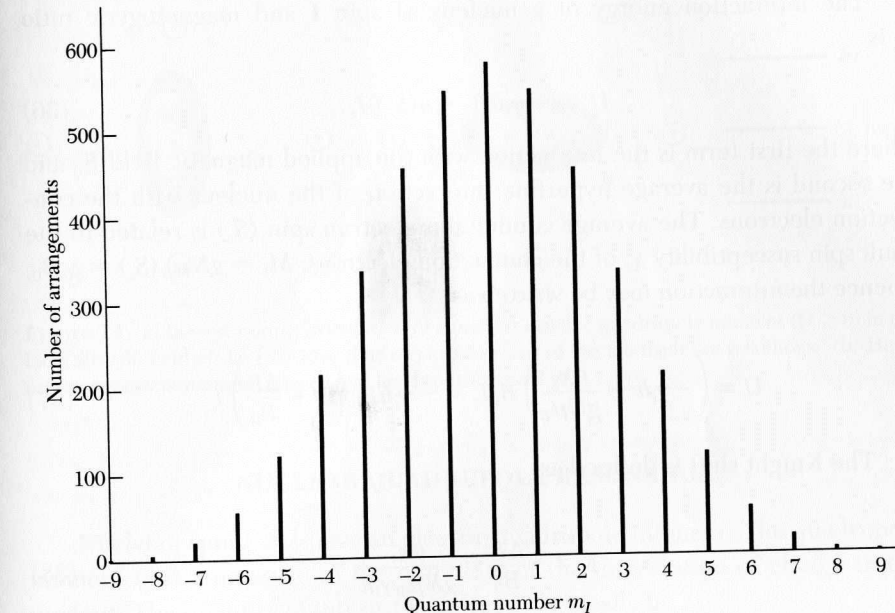


Figure 12 The 4096 arrangements of the six nuclear spins of K^{39} as distributed into 19 hyperfine components. Each component will be split further into a very large number of components by virtue of the residual hyperfine interaction with the 12 neighboring Cl nuclei, which may be Cl^{35} (75 percent) or Cl^{37} (25 percent). The envelope of the pattern is approximately gaussian in form.

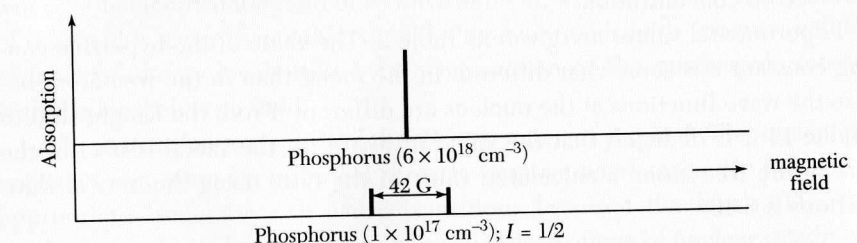


Figure 13 Electron spin resonance lines of P donor atoms in silicon. At the higher donor concentration near the metal-insulator transition, a donor electron can hop from site to site so rapidly that the hyperfine structure is suppressed. (After R. C. Fletcher, W. A. Yager, G. L. Pearson, and F. R. Merritt.)

rapid hopping averages out the hyperfine splitting. The hopping rate increases at the higher concentrations as the overlap of the donor electron wavefunctions is increased, a view supported by conductivity measurements (Chapter 14).

Knight Shift

At a fixed frequency the resonance of a nuclear spin is observed at a slightly different magnetic field in a metal than in a diamagnetic solid. The effect is known as the **Knight shift** or **metallic shift** and is valuable as a tool for the study of conduction electrons.

The interaction energy of a nucleus of spin I and magnetogyric ratio γ_I is

$$U = (-\gamma_I \hbar B_0 + a\langle S_z \rangle) I_z , \quad (36)$$

where the first term is the interaction with the applied magnetic field B_0 and the second is the average hyperfine interaction of the nucleus with the conduction electrons. The average conduction electron spin $\langle S_z \rangle$ is related to the Pauli spin susceptibility χ_s of the conduction electrons: $M_z = gN\mu_B\langle S_z \rangle = \chi_s B_0$, whence the interaction may be written as

$$U = \left(-\gamma_I \hbar + \frac{a\chi_s}{gN\mu_B} \right) B_0 I_z = -\gamma_I \hbar B_0 \left(1 + \frac{\Delta B}{B_0} \right) I_z . \quad (37)$$

The Knight shift is defined as

$$K = -\frac{\Delta B}{B_0} = \frac{a\chi_s}{gN\mu_B\gamma_I\hbar} \quad (38)$$

and simulates a fractional change in the magnetogyric ratio. By the definition (34) of the hyperfine contact energy, the Knight shift is given approximately by $K \approx \chi_s |\psi(0)|^2/N$; that is, by the Pauli spin susceptibility increased in the ratio of the conduction electron concentration at the nucleus to the average conduction electron concentration.

Experimental values are given in Table 2. The value of the hyperfine coupling constant a is somewhat different in the metal than in the free atom because the wave functions at the nucleus are different. From the Knight shift of metallic Li it is deduced that the value of $|\psi(0)|^2$ in the metal is 0.44 of the value in the free atom; a calculated value of the ratio using theoretical wave functions is 0.49.

Table 2 Knight shifts in NMR in metallic elements

(At room temperature)

Nucleus	Knight shift in percent	Nucleus	Knight shift in percent
Li^7	0.0261	Cu^{63}	0.237
Na^{23}	0.112	Rb^{87}	0.653
Al^{27}	0.162	Pd^{105}	-3.0
K^{39}	0.265	Pt^{195}	-3.533
V^{51}	0.580	Au^{197}	1.4
Cr^{53}	0.69	Pb^{207}	1.47

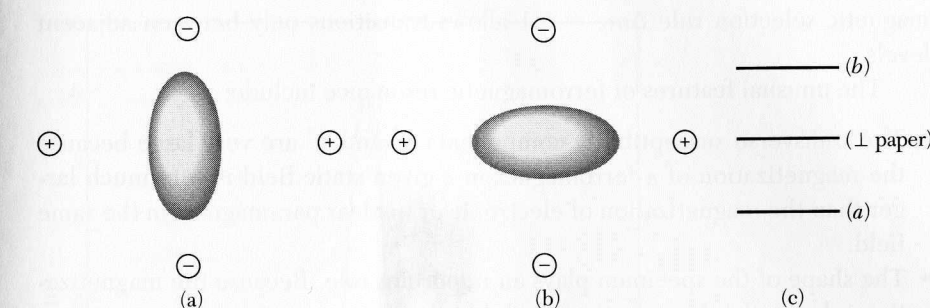


Figure 14 (a) Lowest-energy orientation of a nuclear electric quadrupole moment ($Q > 0$) in the local electric field of the four ions shown. The electrons of the ion itself are not shown. (b) Highest-energy orientation. (c) The energy level splitting for $I = 1$.

NUCLEAR QUADRUPOLE RESONANCE

Nuclei of spin $I \geq 1$ have an electric quadrupole moment. The quadrupole moment Q is a measure of the ellipticity of the distribution of charge in the nucleus. The quantity of interest is defined classically by

$$eQ = \frac{1}{2} \int (3z^2 - r^2)\rho(\mathbf{r})d^3x , \quad (39)$$

where $\rho(\mathbf{r})$ is the charge density. An egg-shaped nucleus has Q positive; a saucer-shaped nucleus has Q negative. The nucleus when placed in a crystal will see the electrostatic field of its environment, as in Fig. 14. If the symmetry of this field is lower than cubic, then the nuclear quadrupole moment will lead to a set of energy levels split by the interaction of the quadrupole moment with the local electric field.

The states that are split are the $2I + 1$ states of a spin I . The quadrupole splittings can often be observed directly because an rf magnetic field of the appropriate frequency can cause transitions between the levels. The term **nuclear quadrupole resonance** refers to observations of nuclear quadrupole splittings in the absence of a static magnetic field. The quadrupole splittings are particularly large in covalently bonded molecules such as Cl_2 , Br_2 , and I_2 ; the splittings are of the order 10^7 or 10^8 Hz.

FERROMAGNETIC RESONANCE

Spin resonance at microwave frequencies in ferromagnets is similar in principle to nuclear spin resonance. The total electron magnetic moment of the specimen precesses about the direction of the static magnetic field, and energy is absorbed strongly from the rf transverse field when its frequency is equal to the precessional frequency. We may think of the macroscopic vector \mathbf{S} representing the total spin of the ferromagnet as quantized in the static magnetic field, with energy levels separated by the usual Zeeman frequencies; the

magnetic selection rule $\Delta m_s = \pm 1$ allows transitions only between adjacent levels.

The unusual features of ferromagnetic resonance include:

- The transverse susceptibility components χ' and χ'' are very large because the magnetization of a ferromagnet in a given static field is very much larger than the magnetization of electronic or nuclear paramagnets in the same field.
- The shape of the specimen plays an important role. Because the magnetization is large, the demagnetization field is large.
- The strong exchange coupling between the ferromagnetic electrons tends to suppress the dipolar contribution to the line width, so that the ferromagnetic resonance lines can be quite sharp (<1 G) under favorable conditions.
- Saturation effects occur at low rf power levels. It is not possible, as it is with nuclear spin systems, to drive a ferromagnetic spin system so hard that the magnetization M_z is reduced to zero or reversed. The ferromagnetic resonance excitation breaks down into spin wave modes before the magnetization vector can be rotated appreciably from its initial direction.

Shape Effects in FMR

We treat the effects of specimen shape on the resonance frequency. Consider a specimen of a cubic ferromagnetic insulator in the form of an ellipsoid with principal axes parallel to x , y , z axes of a cartesian coordinate system. The **demagnetization factors** N_x , N_y , N_z are identical with the depolarization factors to be defined in Chapter 16. The components of the internal magnetic field \mathbf{B}_i in the ellipsoid are related to the applied field by

$$B_x^i = B_x^0 - N_x M_x ; \quad B_y^i = B_y^0 - N_y M_y ; \quad B_z^i = B_z^0 - N_z M_z .$$

The Lorentz field $(4\pi/3)\mathbf{M}$ and the exchange field $\lambda\mathbf{M}$ do not contribute to the torque because their vector product with \mathbf{M} vanishes identically. In SI we replace the components of \mathbf{M} by $\mu_0\mathbf{M}$, with the appropriate redefinition of the N 's.

The components of the spin equation of motion $\dot{\mathbf{M}} = \gamma(\mathbf{M} \times \mathbf{B}^i)$ become, for an applied static field $B_0\hat{z}$,

$$\frac{dM_x}{dt} = \gamma(M_y B_z^i - M_z B_y^i) = \gamma[B_0 + (N_y - N_z)M]M_y ; \quad (40)$$

$$\frac{dM_y}{dt} = \gamma[M(-N_x M_x) - M_x(B_0 - N_z M)] = -\gamma[B_0 + (N_x - N_z)M]M_x .$$

To first order we may set $dM_z/dt = 0$ and $M_z = M$. Solutions of (40) with time dependence $\exp(-i\omega t)$ exist if

$$\begin{vmatrix} i\omega & \gamma[B_0 + (N_y - N_z)M] \\ -\gamma[B_0 + (N_x - N_z)M] & i\omega \end{vmatrix} = 0 ,$$

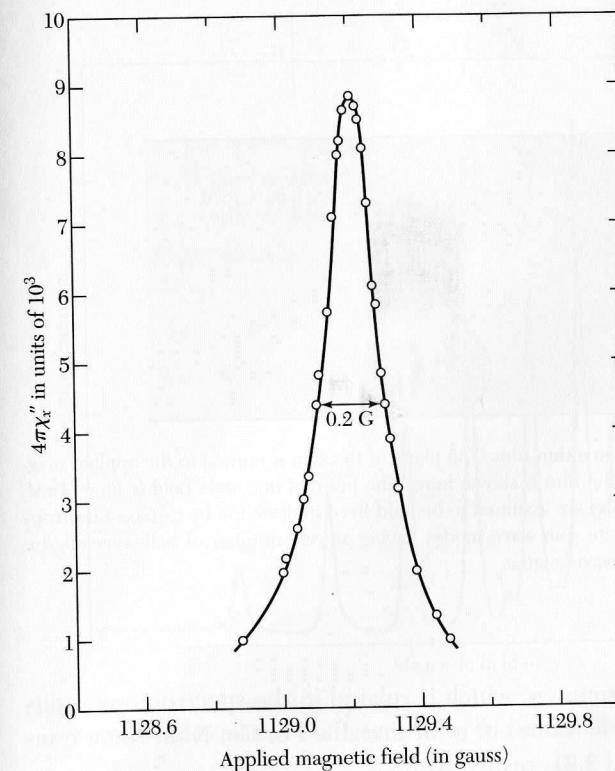


Figure 15 FMR in a polished sphere of the ferromagnet yttrium iron garnet at 3.33 GHz and 300 K for $B_0 \parallel [111]$. The total line width at half-power is only 0.2 G. (After R. C. LeCraw and E. Spencer.)

so that the ferromagnetic resonance frequency in the applied field B_0 is

$$(CGS) \quad \omega_0^2 = \gamma^2[B_0 + (N_y - N_z)M][B_0 + (N_x - N_z)M] ; \quad (41)$$

$$(SI) \quad \omega_0^2 = \gamma^2[B_0 + (N_y - N_z)\mu_0 M][B_0 + (N_x - N_z)\mu_0 M] .$$

The frequency ω_0 is called the frequency of the **uniform mode**, in distinction to the frequencies of magnon and other nonuniform modes. In the uniform mode all the moments precess together in phase with the same amplitude.

For a sphere $N_x = N_y = N_z$, so that $\omega_0 = \gamma B_0$. A very sharp resonance line in this geometry is shown in Fig. 15. For a flat plate with B_0 perpendicular to the plate $N_x = N_y = 0$; $N_z = 4\pi$, whence the ferromagnetic resonance frequency is

$$(CGS) \quad \omega_0 = \gamma(B_0 - 4\pi M) ; \quad (SI) \quad \omega_0 = \gamma(B_0 - \mu_0 M) . \quad (42)$$

If B_0 is parallel to the plane of the plate, the xz plane, then $N_x = N_z = 0$; $N_y = 4\pi$, and

$$(CGS) \quad \omega_0 = \gamma[B_0(B_0 + 4\pi M)]^{1/2} ; \quad (SI) \quad \omega_0 = \gamma[B_0(B_0 + \mu_0 M)]^{1/2} . \quad (43)$$

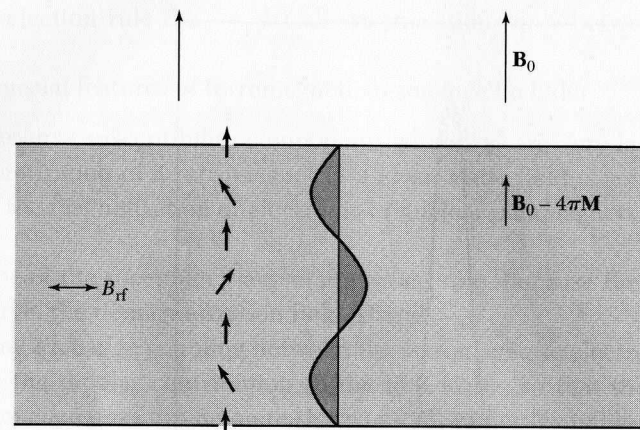


Figure 16 Spin wave resonance in a thin film. The plane of the film is normal to the applied magnetic field B_0 . A cross section of the film is shown here. The internal magnetic field is $B_0 - 4\pi M$. The spins on the surfaces of the film are assumed to be held fixed in direction by surface anisotropy forces. A uniform rf field will excite spin wave modes having an odd number of half-wavelengths. The wave shown is for $n = 3$ half-wavelengths.

The experiments determine γ , which is related to the spectroscopic splitting factor g by $-\gamma = g\mu_B/\hbar$. Values of g for metallic Fe, Co, Ni at room temperature are 2.10, 2.18, and 2.21, respectively.

Spin Wave Resonance

Uniform rf magnetic fields can excite long-wavelength spin waves in thin ferromagnetic films if the electron spins on the surfaces of the film see different anisotropy fields than the spins within the film. In effect, the surface spins may be pinned by surface anisotropy interactions, as shown in Fig. 16. If the rf field is uniform, it can excite waves with an odd number of half-wavelengths within the thickness of the film. Waves with an even number of half-wavelengths have no net interaction energy with the field.

The condition for **spin wave resonance** (SWR) with the applied magnetic field normal to the film is obtained from (42) by adding to the right-hand side the exchange contribution to the frequency. The exchange contribution may be written as Dk^2 , where D is the spin wave exchange constant. The assumption $ka \ll 1$ is valid for the SWR experiments. Thus in an applied field B_0 the spin wave resonance frequencies are:

$$(CGS) \quad \omega_0 = \gamma(B_0 - 4\pi M) + Dk^2 = \gamma(B_0 - 4\pi M) + D(n\pi/L)^2, \quad (44)$$

where the wavevector for a mode of n half-wavelengths in a film of thickness L is $k = n\pi/L$. An experimental spectrum is shown in Fig. 17.

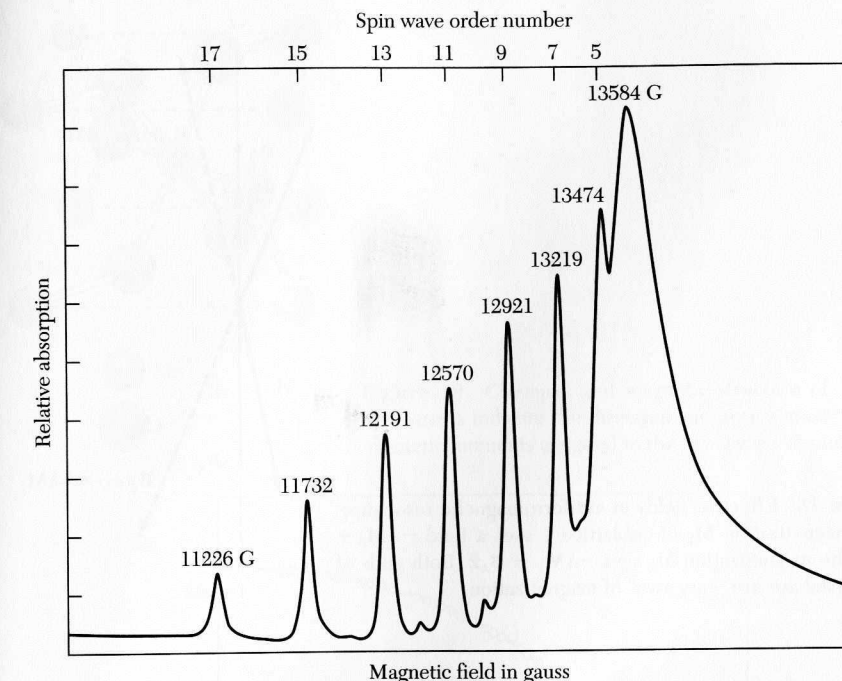


Figure 17 Spin wave resonance spectrum in a Permalloy (80Ni20Fe) film at 9 GHz. The order number is the number of half-wavelengths in the thickness of the film. (After R. Weber.)

ANTIFERROMAGNETIC RESONANCE

We consider a uniaxial antiferromagnet with spins on two sublattices, 1 and 2. We suppose that the magnetization \mathbf{M}_1 on sublattice 1 is directed along the $+z$ direction by an anisotropy field $B_A \hat{\mathbf{z}}$; the anisotropy field (Chapter 12) results from an anisotropy energy density $U_K(\theta_1) = K \sin^2 \theta_1$. Here θ_1 is the angle between \mathbf{M}_1 and the z axis, whence $B_A = 2K/M$, with $M = |\mathbf{M}_1| = |\mathbf{M}_2|$. The magnetization \mathbf{M}_2 is directed along the $-z$ direction by an anisotropy field $-B_A \hat{\mathbf{z}}$. If $+z$ is an easy direction of magnetization, so is $-z$. If one sublattice is directed along $+z$, the other will be directed along $-z$.

The exchange interaction between \mathbf{M}_1 and \mathbf{M}_2 is treated in the mean field approximation. The exchange fields are

$$\mathbf{B}_1(\text{ex}) = -\lambda \mathbf{M}_2; \quad \mathbf{B}_2(\text{ex}) = -\lambda \mathbf{M}_1, \quad (45)$$

where λ is positive. Here \mathbf{B}_1 is the field that acts on the spins of sublattice 1, and \mathbf{B}_2 acts on sublattice 2. In the absence of an external magnetic field the total field acting on \mathbf{M}_1 is $\mathbf{B}_1 = -\lambda \mathbf{M}_2 + B_A \hat{\mathbf{z}}$; the total field on \mathbf{M}_2 is $\mathbf{B}_2 = -\lambda \mathbf{M}_1 - B_A \hat{\mathbf{z}}$, as in Fig. 18.

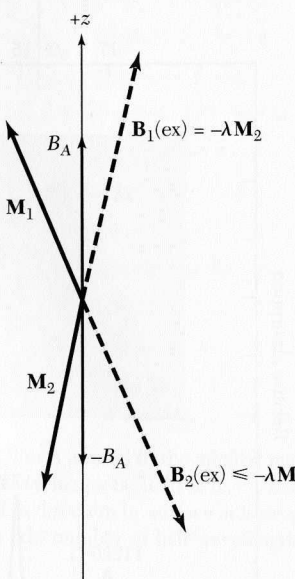


Figure 18 Effective fields in antiferromagnetic resonance. The magnetization \mathbf{M}_1 of sublattice 1 sees a field $-\lambda\mathbf{M}_2 + B_A\hat{\mathbf{z}}$; the magnetization \mathbf{M}_2 sees $-\lambda\mathbf{M}_1 - B_A\hat{\mathbf{z}}$. Both ends of the crystal axis are “easy axes” of magnetization.

In what follows we set $M_1^z = M$; $M_2^z = -M$. The linearized equations of motion are

$$\begin{aligned} dM_1^x/dt &= \gamma[M_1^y(\lambda M + B_A) - M(-\lambda M_2^y)] ; \\ dM_1^y/dt &= \gamma[M(-\lambda M_2^x) - M_1^x(\lambda M + B_A)] ; \end{aligned} \quad (46)$$

$$\begin{aligned} dM_2^x/dt &= \gamma[M_2^y(-\lambda M - B_A) - (-M)(-\lambda M_1^y)] ; \\ dM_2^y/dt &= \gamma[(-M)(-\lambda M_1^x) - M_2^x(-\lambda M - B_A)] . \end{aligned} \quad (47)$$

We define $M_1^+ = M_1^x + iM_1^y$; $M_2^+ = M_2^x + iM_2^y$. Then (46) and (47) become, for time dependence $\exp(-i\omega t)$,

$$\begin{aligned} -i\omega M_1^+ &= -i\gamma[M_1^+(B_A + \lambda M) + M_2^+(\lambda M)] ; \\ -i\omega M_2^+ &= i\gamma[M_2^+(B_A + \lambda M) + M_1^+(\lambda M)] . \end{aligned}$$

These equations have a solution if, with the exchange field $B_E \equiv \lambda M$,

$$\begin{vmatrix} \gamma(B_A + B_E) - \omega & \gamma B_E \\ \gamma B_E & \gamma(B_A + B_E) + \omega \end{vmatrix} = 0 .$$

Thus the antiferromagnetic resonance frequency is given by

$$\omega_0^2 = \gamma^2 B_A (B_A + 2B_E) . \quad (48)$$

MnF_2 is an extensively studied antiferromagnet. The structure is shown in Fig. 19. The observed variation of ω_0 with temperature is shown in Fig. 20. Careful estimates were made by Keffer of B_A and B_E for MnF_2 . He estimated

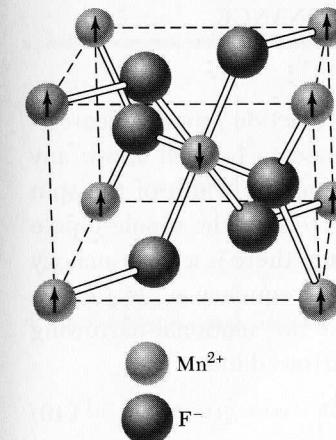


Figure 19 Chemical and magnetic structure of MnF_2 . The arrows indicate the direction and arrangement of the magnetic moments assigned to the manganese atoms.

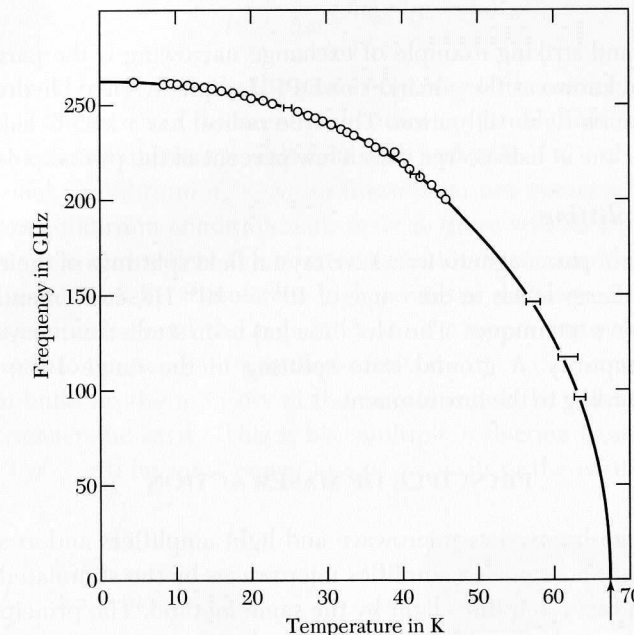


Figure 20 Antiferromagnetic resonance frequency for MnF_2 versus temperature. (After Johnson and Nethercot.)

$B_E = 540$ kG and $B_A = 8.8$ kG at 0 K, whence $(2B_A B_E)^{1/2} = 100$ kG. The observed value is 93 kG.

Richards has made a compilation of AFMR frequencies as extrapolated to 0 K:

Crystal	CoF_2	NiF_2	MnF_2	FeF_2	MnO	NiO
Frequency in 10^{10} Hz	85.5	93.3	26.0	158.	82.8	109

ELECTRON PARAMAGNETIC RESONANCE

Exchange Narrowing

We consider a paramagnet with an exchange interaction J among nearest-neighbor electron spins. The temperature is assumed to be well above any spin-ordering temperature T_c . Under these conditions the width of the spin resonance line is usually much narrower than expected for the dipole-dipole interaction. The effect is called **exchange narrowing**; there is a close analogy with motional narrowing. We interpret the exchange frequency $\omega_{\text{ex}} \approx J/\hbar$ as a hopping frequency $1/\tau$. Then by generalization of the motional-narrowing result (28) we have for the width of the exchange-narrowed line:

$$\Delta\omega \approx (\Delta\omega)_0^2/\omega_{\text{ex}} , \quad (49)$$

where $(\Delta\omega)_0^2 = \gamma^2 \langle B_i^2 \rangle$ is the square of the static dipolar width in the absence of exchange.

A useful and striking example of exchange narrowing is the paramagnetic organic crystal known as the *g* marker or DPPH, diphenyl picryl hydrazyl, often used for magnetic field calibration. This free radical has a 1.35 G half-width of the resonance line at half-power, only a few percent of the pure dipole width.

Zero-Field Splitting

A number of paramagnetic ions have crystal field splittings of their magnetic ground state energy levels in the range of $10^{10} - 10^{11}$ Hz, conveniently accessible by microwave techniques. The Mn^{2+} ion has been studied in many crystals as an additive impurity. A ground state splitting in the range $10^7 - 10^9$ Hz is observed, according to the environment.

PRINCIPLE OF MASER ACTION

Crystals can be used as microwave and light amplifiers and as sources of coherent radiation. A **maser** amplifies microwaves by the stimulated emission of radiation; a **laser** amplifies light by the same method. The principle, due to Townes, may be understood from the two-level magnetic system of Fig. 21 relevant for masers. There are n_u atoms in the upper state and n_l atoms in the lower state. We immerse the system in radiation at frequency ω ; the amplitude of the magnetic component of the radiation field is B_{rf} . The probability per atom per unit time of a transition between the upper and lower states is

$$P = \left(\frac{\mu B_{\text{rf}}}{\hbar} \right)^2 \frac{1}{\Delta\omega} ; \quad (50)$$

here μ is the magnetic moment, and $\Delta\omega$ is the combined width of the two levels. The result (50) is from a standard result of quantum mechanics, called Fermi's golden rule.

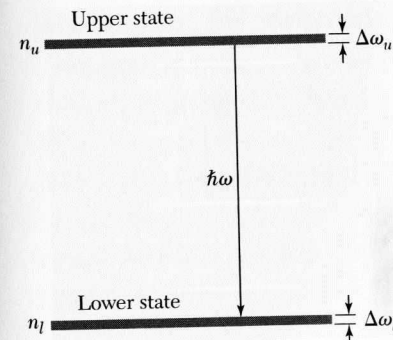


Figure 21 A two-level system, to explain maser operation. The populations of the upper and lower states are n_u and n_l , respectively. The frequency of the emitted radiation is ω ; the combined width of the states is $\Delta\omega = \Delta\omega_u + \Delta\omega_l$.

The net energy emitted from atoms in both upper and lower states is

$$\mathcal{P} = \left(\frac{\mu B_{\text{rf}}}{\hbar} \right)^2 \frac{1}{\Delta\omega} \cdot \hbar\omega \cdot (n_u - n_l) , \quad (51)$$

per unit time. Here \mathcal{P} denotes the power out; $\hbar\omega$ is the energy per photon; and $n_u - n_l$ is the excess of the number of atoms n_u initially able to emit a photon over the number of atoms n_l able to absorb a photon.

In thermal equilibrium $n_u < n_l$, so there is no net emission of radiation, but in a nonequilibrium condition with $n_u > n_l$ there will be emission. If we start with $n_u > n_l$ and reflect the emitted radiation back onto the system, we increase B_{rf} and thereby stimulate a higher rate of emission. The enhanced stimulation continues until the population in the upper state decreases and becomes equal to the population in the lower state.

We can build up the intensity of the radiation field by placing the crystal in an electromagnetic cavity. This is like multiple reflection from the walls of the cavity. There will be some power loss in the walls of the cavity: the rate of power loss is

$$(CGS) \quad \mathcal{P}_L = \frac{B_{\text{rf}}^2 V}{8\pi} \cdot \frac{\omega}{Q} ; \quad (SI) \quad \mathcal{P}_L = \frac{B_{\text{rf}}^2}{2\mu_0} \cdot \frac{\omega}{Q} , \quad (52)$$

where V is the volume and Q is the Q factor of the cavity. We understand B_{rf}^2 to be a volume average.

The condition for maser action is that the emitted power \mathcal{P} exceed the power loss \mathcal{P}_L . Both quantities involve B_{rf}^2 . The maser condition can now be expressed in terms of the population excess in the upper state:

$$(CGS) \quad n_u - n_l > \frac{V\Delta B}{8\pi\mu Q} , \quad (SI) \quad n_u - n_l > \frac{V\Delta B}{2\mu_0\mu Q} , \quad (53)$$

where μ is the magnetic moment. The line width ΔB is defined in terms of the combined line width $\Delta\omega$ of the upper and lower states as $\mu\Delta B = \hbar\Delta\omega$. The

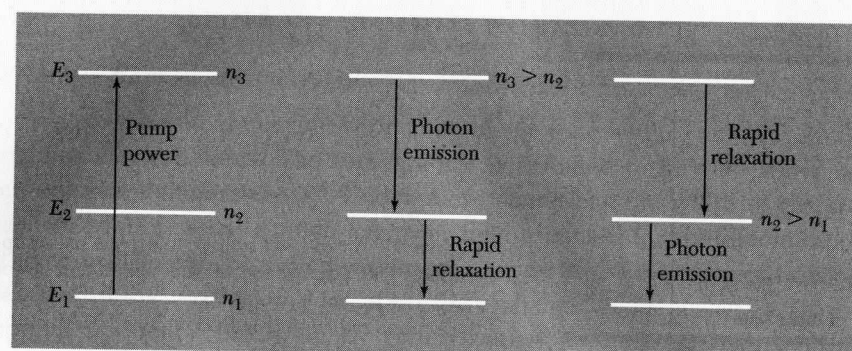


Figure 22 Three-level maser system. Two possible modes of operation are shown, starting from rf saturation of the states 3 and 1 to obtain $n_3 = n_1$.

central problem of the maser or laser is to obtain a suitable excess population in the upper state. This is accomplished in various ways in various devices.

Three-Level Maser

The three-level maser system (Fig. 22) is a clever solution to the excess population problem. Such a system may derive its energy levels from magnetic ions in a crystal, as Bloembergen showed. Rf power is applied at the pump frequency $\hbar\omega_p = E_3 - E_1$ in sufficient intensity to maintain the population of level 3 substantially equal to the population of level 1. This is called saturation—see Problem 6. Now consider the rate of change of the population n_2 of level 2 owing to normal thermal relaxation processes. In terms of the indicated transition rates P ,

$$\frac{dn_2}{dt} = -n_2 P(2 \downarrow 1) - n_2 P(2 \downarrow 3) + n_3 P(3 \downarrow 2) + n_1 P(1 \downarrow 2). \quad (54)$$

In the steady state $\frac{dn_2}{dt} = 0$, and by virtue of the saturation rf power we have $n_3 = n_1$, whence

$$\frac{n_2}{n_1} = \frac{P(3 \downarrow 2) + P(1 \downarrow 2)}{P(2 \downarrow 1) + P(2 \downarrow 3)}. \quad (55)$$

The transition rates are affected by many details of the paramagnetic ion and its environment, but one can hardly fail with this system, for either $n_2 > n_1$ and we get maser action between levels 2 and 1, or $n_2 < n_1 = n_3$ and we get maser action between levels 3 and 2. The energy levels of the Er^{3+} ion are used in communication fiber optics amplifiers. The ion is optically pumped from level 1 to level 3; there is fast nonradiative decay from level 3 to level 2. The signal at a wavelength of $1.55 \mu\text{m}$ is amplified by stimulated emission from level 2 to level 1. The wavelength is favorable for long-distance propagation in the optical fiber. The bandwidth is of the order of $4 \times 10^{12} \text{ Hz}$.

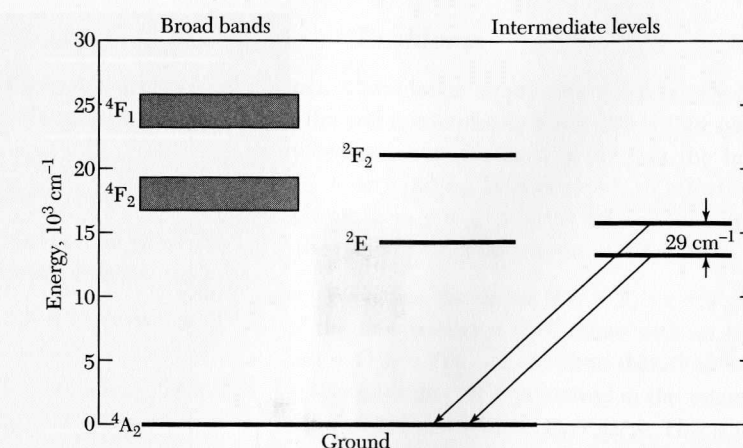


Figure 23 Energy level diagram of Cr^{3+} in ruby, as used in laser operation. The initial excitation takes place to the broad bands; they decay to the intermediate levels by the emission of phonons, and the intermediate levels radiate photons as the ion makes the transition to the ground level.

Lasers

The same crystal, ruby, used in the microwave maser was also the first crystal to exhibit optical maser action, but a different set of energy levels of Cr^{3+} are involved (Fig. 23). About $15,000 \text{ cm}^{-1}$ above the ground state there lie a pair of states labeled 2E , spaced 29 cm^{-1} apart. Above 2E lie two broad bands of states, labeled 4F_1 and 4F_2 . Because the bands are broad they can be populated efficiently by optical absorption from broadband light sources such as xenon flash lamps.

In operation of a ruby laser both of the broad 4F bands are populated by broadband light. Atoms thus excited will decay in 10^{-7} sec by radiationless processes with the emission of phonons to the states 2E . Photon emission from the lower of the states 2E to the ground state occurs slowly, in about $5 \times 10^{-3} \text{ sec}$, so that a large excited population can pile up in 2E . For laser action this population must exceed that in the ground state.

The stored energy in ruby is 10^8 erg cm^{-3} if 10^{20} Cr^{3+} ions cm^{-3} are in an excited state. The ruby laser can emit at a very high power level if all this stored energy comes out in a short burst. The overall efficiency of conversion of a ruby laser from input electrical energy to output laser light is about one percent. Another popular solid state laser is the neodymium glass laser, made of calcium tungstate glass doped with Nd^{3+} ions. This operates as a four level system (Fig. 24). Here it is not necessary to empty out the ground state before laser action can occur.

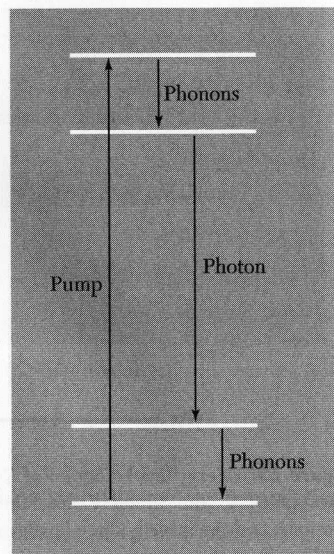


Figure 24 Four-level laser system, as in the neodymium glass laser.

SUMMARY

(In CGS Units)

- The resonance frequency of a free spin is $\omega_0 = \gamma B_0$, where $\gamma = \mu/\hbar I$ is the magnetogyric ratio.
- The Bloch equations are
$$dM_x/dt = \gamma(\mathbf{M} \times \mathbf{B})_x - M_x/T_2 ;$$

$$dM_y/dt = \gamma(\mathbf{M} \times \mathbf{B})_y - M_y/T_2 ;$$

$$dM_z/dt = \gamma(\mathbf{M} \times \mathbf{B})_z + (M_0 - M_z)/T_1 .$$
- The half-width of the resonance at half-power is $(\Delta\omega)_{1/2} = 1/T_2$.
- The dipolar line width in a rigid lattice is $(\Delta B)_0 \approx \mu/a^3$.
- If the magnetic moments are ambulatory, with a characteristic time $\tau \ll 1/(\Delta\omega)_0$, the line width is reduced by the factor $(\Delta\omega)_0\tau$. In this limit $1/T_1 \approx 1/T_2 \approx (\Delta\omega)_0^2\tau$. With exchange coupling in a paramagnet the line width becomes $\approx (\Delta\omega)_0^2\omega_{ex}$.
- The ferromagnetic resonance frequency in an ellipsoid of demagnetization factors N_x, N_y, N_z is $\omega_0^2 = \gamma^2[B_0 + (N_y - N_z)M][B_0 + (N_x - N_z)M]$.
- The antiferromagnetic resonance frequency is $\omega_0^2 = \gamma^2B_A(B_A + 2B_E)$, in a spherical specimen with zero applied field. Here B_A is the anisotropy field and B_E is the exchange field.
- The condition for maser action is that $n_u - n_l > V\Delta B/8\pi\mu Q$.

Problems

- Equivalent electrical circuit.** Consider an empty coil of inductance L_0 in a series with a resistance R_0 ; show if the coil is completely filled with a spin system characterized by the susceptibility components $\chi'(\omega)$ and $\chi''(\omega)$ that the inductance at frequency ω becomes $L = [1 + 4\pi\chi'(\omega)]L_0$, in series with an effective resistance $R = 4\pi\omega\chi''(\omega)L_0 + R_0$. In this problem $\chi = \chi' + i\chi''$ is defined for a linearly polarized rf field. Hint: Consider the impedance of the circuit. (CGS units.)
- Rotating coordinate system.** We define the vector $\mathbf{F}(t) = F_x(t)\hat{\mathbf{x}} + F_y(t)\hat{\mathbf{y}} + F_z(t)\hat{\mathbf{z}}$. Let the coordinate system of the unit vectors $\hat{\mathbf{x}}, \hat{\mathbf{y}}, \hat{\mathbf{z}}$ rotate with an instantaneous angular velocity Ω , so that $d\hat{\mathbf{x}}/dt = \Omega_y\hat{\mathbf{z}} - \Omega_z\hat{\mathbf{y}}$, etc. (a) Show that $d\mathbf{F}/dt = (d\mathbf{F}/dt)_R + \Omega \times \mathbf{F}$, where $(d\mathbf{F}/dt)_R$ is the time derivative of \mathbf{F} as viewed in the rotating frame R . (b) Show that (7) may be written $(d\mathbf{M}/dt)_R = \gamma\mathbf{M} \times (\mathbf{B}_a + \Omega/\gamma)$. This is the equation of motion of \mathbf{M} in a rotating coordinate system. The transformation to a rotating system is extraordinarily useful; it is exploited widely in the literature. (c) Let $\Omega = -\gamma B_0 \hat{\mathbf{z}}$; thus in the rotating frame there is no static magnetic field. Still in the rotating frame, we now apply a dc pulse $B_1 \hat{\mathbf{x}}$ for a time t . If the magnetization is initially along $\hat{\mathbf{z}}$, find an expression for the pulse length t such that the magnetization will be directed along $-\hat{\mathbf{z}}$ at the end of the pulse. (Neglect relaxation effects.) (d) Describe this pulse as viewed from the laboratory frame of reference.
- Hyperfine effects on ESR in metals.** We suppose that the electron spin of a conduction electron in a metal sees an effective magnetic field from the hyperfine interaction of the electron spin with the nuclear spin. Let the z component of the field seen by the conduction electron be written
$$B_i = \left(\frac{a}{N}\right) \sum_{j=1}^N I_j^z ,$$

where I_j^z is equally likely to be $\pm \frac{1}{2}$. (a) Show that $\langle B_i^3 \rangle = (a/2N)^2 N$. (b) Show that $\langle B_i^4 \rangle = 3(a/2N)^4 N^2$, for $N \gg 1$.

- FMR in the anisotropy field.** Consider a spherical specimen of a uniaxial ferromagnetic crystal with an anisotropy energy density of the form $U_K = K \sin^2 \theta$, where θ is the angle between the magnetization and the z axis. We assume that K is positive. Show that the ferromagnetic resonance frequency in an external magnetic field $B_0 \hat{\mathbf{z}}$ is $\omega_0 = \gamma(B_0 + B_A)$, where $B_A = 2K/M_s$.
- Exchange frequency resonance.** Consider a ferrimagnet with two sublattices A and B of magnetizations \mathbf{M}_A and \mathbf{M}_B , where \mathbf{M}_B is opposite to \mathbf{M}_A when the spin system is at rest. The gyromagnetic ratios are γ_A, γ_B and the molecular fields are $\mathbf{B}_A = -\lambda \mathbf{M}_B; \mathbf{B}_B = -\lambda \mathbf{M}_A$. Show that there is a resonance at
$$\omega_0^2 = \lambda^2(\gamma_A|M_B| - \gamma_B|M_A|)^2 .$$

This is called the exchange frequency resonance.

- Rf saturation.** Given, at equilibrium for temperature T , a two-level spin system in a magnetic field $H_0 \hat{\mathbf{z}}$, with populations N_1, N_2 and transition rates W_{12}, W_{21} . We

apply an rf signal that gives a transition rate W_{rf} . (a) Derive the equation for dM_z/dt and show that in the steady state

$$M_z = M_0/(1 + 2W_{rf}T_1) ,$$

where $1/T_1 = W_{12} + W_{21}$. It will be helpful to write $N = N_1 + N_2$; $n = N_1 - N_2$; and $n_0 = N(W_{21} - W_{12})/(W_{21} + W_{12})$. We see that as long as $2W_{rf}T_1 \ll 1$ the absorption of energy from the rf field does not substantially alter the population distribution from its thermal equilibrium value. (b) Using the expression for n , write down the rate at which energy is absorbed from the rf field. What happens as W_{rf} approaches $1/2T_1$? This effect is called saturation, and its onset may be used to measure T_1 .

14

Plasmons, Polaritons, and Polaron

DIELECTRIC FUNCTION OF THE ELECTRON GAS	395
Definitions of the dielectric function	395
Plasma optics	396
Dispersion relation for electromagnetic waves	397
Transverse optical modes in a plasma	398
Transparency of metals in the ultraviolet	398
Longitudinal plasma oscillations	398
PLASMONS	401
ELECTROSTATIC SCREENING	403
Screened coulomb potential	406
Pseudopotential component $U(0)$	407
Mott metal-insulator transition	407
Screening and phonons in metals	409
POLARITONS	410
LST relation	414
ELECTRON-ELECTRON INTERACTION	417
Fermi liquid	417
Electron-electron collisions	417
ELECTRON-PHONON INTERACTION: POLARONS	420
PEIERLS INSTABILITY OF LINEAR METALS	422
SUMMARY	424
PROBLEMS	424
1. Surface plasmons	424
2. Interface plasmons	425
3. Alfvén waves	425

NOTE: The text and problems of this chapter assume facility in the use of electromagnetic theory at the level of a good senior course.